JEE Journal of Ecological Engineering

*Journal of Ecological Engineering*, 2026, 27(10), 367–382
https://doi.org/10.12911/22998993/225466
ISSN 2299–8993, License CC-BY 4.0

Received: 2026.06.27
Accepted: 2026.08.14
Published: 2026.09.01

# Microstructural evolution of aluminosilicate binder under varying thermal conditions

Farangiz Sabirova[1*], Sherzod Matchanov[1], Gulnoza Kodirova[2], Kutligul Kudiyarova[3], Aida Ruzmetova[1]

[1]Urgench State University named after Abu Rayhon Biruni, 220100 Urgench, Uzbekistan
[2]Namangan State Technical University, 160100 Namangan, Uzbekistan
[3]Karakalpak State University named after Berdakh, 230112 Nukus, Uzbekistan
*Corresponding author's e-mail: farangiz2094@icloud.com

## ABSTRACT

This study investigates the structural evolution of aluminosilicate clinker synthesized from a multicomponent raw material system consisting of kaolin, limestone, ceramic brick waste, and liquid glass, heat-treated at 600 °C and 1000 °C. The primary objective was to establish the relationship between firing temperature, phase composition, and microstructural development in the clinker system. A comprehensive physicochemical characterization was performed using X-ray fluorescence spectroscopy (XRF), differential thermal and thermogravimetric analysis (DTA/TG), Fourier transform infrared spectroscopy (FTIR), X-ray diffraction microscopy (XRD), and scanning electron microscopy combined with energy dispersive spectroscopy (EDS/SEM). Experimental results showed that increasing the firing temperature gradually promoted dehydration, decarbonization, and significant restructuring of the aluminosilicate framework. At 600 °C, the material remained predominantly amorphous in nature and retained residual hydroxyl phases, indicating incomplete thermal activation. In contrast, firing at 1000 °C induced the formation of well-defined crystalline phases, including wollastonite ($CaSiO_3$) and akermanite ($Ca_2MgSi_2O_7$), accompanied by increased phase stability and noticeable microstructural compaction. A comparative analysis of the two thermal regimes revealed a clear transition from a partially activated, disordered aluminosilicate system to a more ordered, thermally stable clinker structure with improved physicochemical properties. The obtained results provide new insights into the mechanistic pathways of aluminosilicate clinker formation during thermal activation and confirm the feasibility of using local mineral resources of the Aral Sea region for the production of heat-resistant and environmentally sustainable binders.

**Keywords:** aluminosilicate clinker; thermal analysis; phase transformations; dehydration; temperature; optimal sample.

## INTRODUCTION

### Aluminosilicate materials and binder systems

Aluminosilicate materials are widely used as raw materials in cement binders, ceramics, refractories, and alkali-activated systems. Their importance stems from the presence of reactive silica and alumina phases capable of forming strong binder structures after thermal or chemical activation. The fundamental principles of geopolymer formation from aluminosilicate materials were established in early studies [1], and subsequent studies emphasized the critical role of precursor composition and activation conditions in binder performance [2]. Geopolymer binders have been identified as promising sustainable alternatives to Portland cement [3], and their favorable mechanical and thermal properties—resulting from the formation of stable aluminosilicate networks—have been experimentally confirmed [4].

The properties of aluminosilicate binders depend on the mineralogical composition, phase

structure, and reactivity of the clinker. Optimization of the chemical composition and firing conditions has been shown to significantly affect the development of strength and durability [5,6]. The use of modern microstructural analysis methods, including X-ray diffraction, scanning electron microscopy, and thermal analysis, has significantly improved our understanding of phase formation processes in cementite systems [7,8]. In this context, the study of structural transformations in aluminosilicate materials remains an important and relevant scientific task.

## Environmental challenges and sustainable binder development

High energy demands and significant carbon dioxide emissions associated with conventional cement production have increased interest in sustainable binder technologies [9]. Recent studies have shown that geopolymer and alkali-activated aluminosilicate materials can reduce environmental impacts while maintaining satisfactory mechanical and durability properties [10,11]. At the same time, the incorporation of industrial waste and recycled mineral resources into binder systems promotes resource efficiency and waste reduction [12]. These results suggest that alkali-activated and geopolymer materials based on aluminosilicate raw materials represent a promising route to more sustainable building materials [13,14].

## Utilization of ceramic waste and circular economy principles

The potential of fly ash as a reactive aluminosilicate precursor has been demonstrated in previous studies, highlighting its suitability for the production of binders [15]. The positive effects of silica-containing additives on the physicomechanical properties of cementite systems have also been reported in a number of studies [16–23]. Subsequently, the feasibility of using industrial waste in geopolymer materials has been confirmed [24], and the suitability of different fly ash ashes as geopolymer precursors has been assessed through comparative analysis [25]. The production of heat-resistant binders from local raw materials has also been investigated [26], and further development of secondary mineral resources for the production of sodium silicates is presented in [27]. It has also been shown that calcium-containing additives can significantly improve the mechanical properties of fly ash-based geopolymer systems [28].

## Thermal treatment and phase evolution of aluminosilicate systems

Thermal activation of aluminosilicate materials is accompanied by a series of physicochemical transformations. The thermal behavior and decomposition kinetics of kaolinite have been studied in detail, showing that dehydroxylation plays a crucial role in the formation of reactive phases [29]. Further studies of metakaolin geopolymers showed that increasing temperature affects phase stability and structural development [30], and the formation of ceramic phases from heat-treated metakaolin-based geopolymers was subsequently confirmed [31,32]. Mechanical and thermal characterization of silicate-activated aluminosilicate systems revealed the importance of heat treatment for the overall material performance [33]. The microstructural evolution occurring during geopolymerization was described using SEM and XRD analyses [34]. Thermal stability of geopolymer materials exposed to high temperatures has also been reported [35], and similar observations have been made on the effects of high temperatures on geopolymer pastes, mortars and concretes, including studies of thermal damage mechanisms in geopolymer composites [36,37]. Furthermore, the curing temperature has been shown to significantly influence the development of the structure of the hardened geopolymer [38].

## Research gap and unresolved issues

The structural aspects of geopolymer gels have been studied in detail, providing valuable information on the arrangement of aluminosilicate networks [39]. The influence of composition on the characteristics and structure of alkali-activated metakaolin-slag systems has also been studied [40]. The influence of solid-to-liquid ratios and activators on the formation and properties of geopolymers has been studied in subsequent studies [41], and the potential of geopolymer foam concrete for sustainable construction has been demonstrated [42].

The mechanical and microstructural characteristics of geopolymer cements made from natural aluminosilicate materials have been reported in the literature [43]. Furthermore, approaches to

enhancing the reactivity of aluminosilicate precursors for geopolymer synthesis have been reviewed and systematized [44].

### Novelty, objectives and ecological significance of the study

The properties of cementitious materials and the role of phase composition in binder formation were reported by Makarova et al. [45]. The composition and processing potential of Khojakul kaolin were investigated by Yaqubov et al. [46], while Matchanov et al. [47,48] studied methods for improving its quality. The formation of alkali-activated materials from thermally treated mineral raw materials was demonstrated by Mintsaev et al. [49]. Despite these advances, the influence of firing temperature on the structural evolution of aluminosilicate clinker remains insufficiently understood. Therefore, this study investigates the effect of thermal treatment on the phase composition and microstructure of an optimal aluminosilicate clinker. Despite these achievements, limited attention has been paid to the structural evolution of aluminosilicate clinker during heat treatment and the relationship between firing temperature, phase formation, and microstructure development. Therefore, further research is needed to clarify the influence of thermal activation on clinker structure and properties.

## MATERIALS AND METHODS

### Raw materials and sample preparation

The raw materials used in this study included kaolin, limestone, ceramic waste, and liquid glass. Prior to sample preparation, kaolin, limestone, and ceramic waste were dried and ground using a laboratory ball mill. The obtained powders were sieved through a 0.6 mm sieve to ensure particle size uniformity.

Based on the compositions presented in Table 1, the raw materials were thoroughly mixed and homogenized. Liquid glass was gradually added to the dry mixture until a uniform mass was obtained. The prepared samples were dried at room temperature and subsequently subjected to thermal treatment at 600 °C and 1000 °C. The holding time at the target temperature was 5 h. After cooling to room temperature, the clinker samples were used for physicochemical characterization.

The calcination temperatures of 600 °C and 1000 °C were chosen based on thermal analysis results obtained from preliminary DTA/TG studies, which identified these temperatures as representing two distinct activation states: an intermediate, partially activated state at 600 °C and a fully developed crystalline phase assembly at 1000 °C. This approach is consistent with previous studies of thermally activated aluminosilicate systems [29,30], which have demonstrated that the most significant structural transformations occur below 600 °C and above 900 °C, with the intermediate range serving primarily as a transition zone.

### X-ray fluorescence analysis

The chemical composition of the raw materials and clinker samples was determined by X-ray fluorescence spectroscopy (XRF) using a Rigaku X-ray fluorescence spectrometer. Measurements were carried out under both vacuum and atmospheric conditions. The vacuum mode was used to improve the detection sensitivity of light elements (Si and Al), whereas heavy elements were analyzed under normal atmospheric conditions using an Rh-anode X-ray tube operated at 50 kV and 40 mA. The samples were prepared in the form of pressed pellets.

Calibration was performed using certified standard reference materials (SRM, NIST). Data acquisition and processing were carried out using Spectra Plus and Shimadzu XRF Manager software packages. This method enabled accurate non-destructive determination of both major and trace elements over a wide concentration range.

### Thermal analysis (DTA/TG)

Thermal analysis of the samples was performed using a NETZSCH STA 449 F3 Jupiter thermal analyzer. Measurements were conducted in the temperature range of 25–1000 °C at a heating rate of 10 °C $min^{-1}$ under a nitrogen atmosphere with a flow rate of 50 mL $min^{-1}$. The sample mass used for each measurement was approximately 10 mg.

### Fourier-transform infrared spectroscopy

Fourier-transform infrared spectroscopy (FTIR) was employed to identify the functional groups and structural changes occurring in the clinker samples. Infrared spectra were recorded

using a Bruker Tensor 27 FTIR spectrometer in the wavenumber range of 4000–400 $cm^{-1}$ with a spectral resolution of 4 $cm^{-1}$. Measurements were performed using the ATR technique equipped with a diamond crystal. For each sample, 32 scans were collected at room temperature.

### X-ray diffraction analysis

The phase composition of the clinker samples was investigated by X-ray diffraction (XRD) using a Rigaku diffractometer with Cu Kα radiation (λ = 1.5406 Å). Diffraction patterns were recorded in the 2θ range of 5–80° at room temperature. Phase identification was performed using the ICDD PDF database.

### Scanning electron microscopy and energy-dispersive spectroscopy

The microstructure and elemental composition of the clinker samples were investigated using scanning electron microscopy (SEM) coupled with energy-dispersive X-ray spectroscopy (EDS). SEM observations were carried out using an Alpha-series scanning electron microscope operating under high-vacuum conditions at an accelerating voltage of 20 kV and a working distance of 5–6 mm. EDS analysis was used to determine the elemental composition of selected regions of the samples.

### Mechanical testing

The compressive strength of aluminosilicate binder specimens was determined using two specimen geometries: cubic specimens measuring 100 × 100 × 100 mm and prismatic specimens measuring 150 × 600 mm. Specimens were maintained at room temperature (20 ± 2 °C) under ambient humidity conditions for 1, 7, 14, and 28 days. Tests were conducted using a hydraulic press in accordance with EN 196-1. Each data point represents the average value of three parallel specimens.

## RESULTS AND DISCUSSIONS

### Chemical composition of the raw mixtures

The optimal composition of the aluminosilicate clinker was determined by systematically varying the proportions of kaolin, limestone, ceramic brick waste, and liquid glass. Four experimental mixtures, designated ASB-1 through ASB-4, were prepared and evaluated for their chemical and phase-forming properties. The compositions of all studied samples are summarized in Table 1.

The raw materials were selected to provide the necessary sources of silica ($SiO_2$), alumina ($Al_2O_3$), and calcium oxide (CaO) required for clinker phase formation during high-temperature processing. Kaolin served as the main aluminosilicate component, providing both $SiO_2$ and $Al_2O_3$ as important network-forming oxides. Limestone served as the main calcium-containing component, facilitating the formation of calcium silicate and aluminate mineral phases during firing. Ceramic brick waste was included as an additional source of aluminosilicates, which simultaneously promotes resource efficiency and supports sustainable materials development principles through the recycling of production byproducts. Liquid glass (sodium silicate solution) was used as an alkaline activator and binding agent, facilitating the physicochemical interaction of the raw material components and enhancing the adhesion of the green bodies prior to heat treatment.

Systematic analysis of the experimental data showed that varying the component proportions significantly affects the phase composition and microstructural development of the resulting clinker. Among the four compositions studied,

**Table 1.** Composition of the raw mixture for obtaining aluminosilicate clinker

| Raw material name | Samples, wt.% (mass %) | | | |
|---|---|---|---|---|
| | ASB-1 | ASB-2 | ASB-3 | ASB-4 |
| Kaolin | 35 | 37 | 39 | 40 |
| Limestone | 19 | 18 | 15 | 20 |
| Ceramic waste | 27 | 27 | 30 | 20 |
| Liquid glass | 19 | 18 | 16 | 20 |
| Total, % | 100 | 100 | 100 | 100 |

sample ASB-3—containing 39 wt.% kaolin, 15 wt.% limestone, 30 wt.% ceramic brick waste, and 16 wt.% liquid glass—demonstrated the most thermodynamically balanced ratio of aluminosilicate to calcium-containing components. This compositional equilibrium is considered critical for facilitating the formation of well-defined crystalline phases during firing. Therefore, sample ASB-3 was selected as the reference optimal mixture for all subsequent thermal, mineralogical, and microstructural characterizations.

The selection of ASB-3 as the optimal composition was based on quantitative comparison of all four mixtures fired at 1000 °C Table 2. ASB-3 demonstrated the highest 28-day compressive strength of 15.4 MPa, the lowest total mass loss of 8–12 wt.% indicating more complete thermal activation, and the most well-defined crystalline phase assemblage consisting of wollastonite and akermanite.

Although ASB-4 showed relatively close mechanical performance (13.5 MPa), its XRD pattern revealed a less mature phase composition with residual amorphous content. Compositions ASB-1 and ASB-2 exhibited notably higher mass losses and lower strength values, confirming insufficient thermochemical equilibrium under the applied firing conditions. Therefore, ASB-3 was selected as the reference optimal mixture for all subsequent characterizations.

## X-ray fluorescence analysis of aluminosilicate clinker fired at 600 °C

The elemental composition of the optimal aluminosilicate clinker sample fired at 600 °C was determined using X-ray fluorescence spectroscopy (XRF) (Figure 1). The resulting spectrum revealed that the material is primarily composed of silicon, aluminum, and calcium, confirming the establishment of a well-defined aluminosilicate-based system. The chemical composition of the optimal aluminosilicate clinker sample fired at 600 °C was investigated by X-ray fluorescence (XRF) analysis (Figure 1).

Silicon and aluminum were identified as the main constituent elements, with concentrations reaching approximately 55 wt.% and 30 wt.%, respectively. This compositional profile indicates the presence of a well-developed aluminosilicate framework and creates favorable thermochemical conditions for subsequent phase transformations during further heat treatment. The calculated Si/Al molar ratio of approximately 2.0–2.5 reflects sufficient chemical reactivity of the precursor material

**Table 2.** Comparative characteristics of aluminosilicate binder compositions fired at 1000 °C

| Sample | 28-day compressive strength (MPa) | DTA/TG mass loss (wt.%) | Main XRD phases (1000 °C) |
|---|---|---|---|
| ASB-1 | 11.2 | 14–17 | Amorphous + quartz + residual carbonate |
| ASB-2 | 12.8 | 13–15 | Amorphous + quartz + minor wollastonite |
| ASB-3 | 15.4 | 8–12 | Wollastonite + Akermanite (well-defined) |
| ASB-4 | 13.5 | 12–14 | Quartz + minor wollastonite + amorphous |

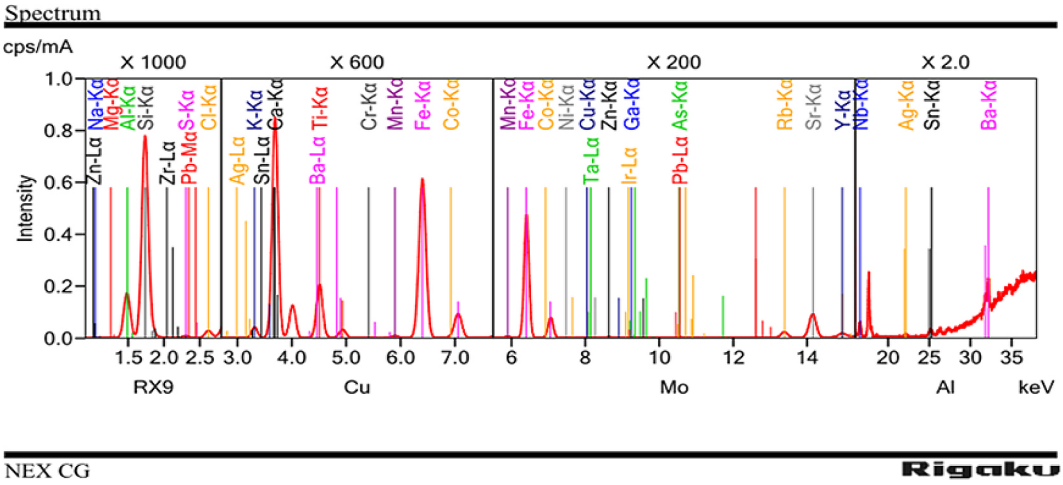


**Figure 1.** X-ray fluorescence (XRF) analysis of clinker samples fired at 600 °C

and is considered favorable for the formation of stable aluminosilicate phases at elevated temperatures.

Calcium was detected in moderate concentrations (up to 12 wt%), indicating the active participation of limestone-derived components in clinker formation reactions. Trace amounts of iron and alkaline elements were also detected in the spectrum. These additional components are known to influence the formation of secondary mineral phases and promote the development of an amorphous glassy matrix in the clinker microstructure. Taken together, the XRF results confirm that the selected raw material composition provides the necessary chemical conditions for the formation of heat-resistant aluminosilicate clinker during subsequent high-temperature processing.

## Thermal behavior of aluminosilicate clinker pre-calcined at 600 °C – DTA/TG analysis

The thermal behavior of an optimal aluminosilicate clinker sample pre-calcined at 600 °C was studied by simultaneous differential thermal analysis and thermogravimetry (DTA/TG). The resulting thermogram is shown in Figure 2. Several characteristic thermal phenomena have been identified, each of which reflects various phase and structural transformations occurring in the material during progressive heating.

In the low temperature range (up to about 150 °C), a pronounced endothermic effect was recorded, accompanied by a maximum mass loss of about 0.5–1.0 wt.%. This thermal reaction is due to the elimination of physically adsorbed moisture and residual pore water retained in the clinker microstructure.

In the intermediate temperature range of about 150–350 °C, a relatively weak endothermic process was detected, corresponding to the removal of chemically bound water and the onset of dehydroxylation of the hydrated aluminosilicate phases. The accompanying weight loss in this range was about 1–2 wt.%.

The most pronounced thermal effect was observed in the 400–650 °C range, where a broad endothermic peak was recorded in the DTA curve. This feature is due to the progressive dehydroxylation of aluminosilicate clay minerals, accompanied by the destruction of their ordered crystalline structure and a transition to a reactive amorphous metakaolin-like state. The cumulative mass loss associated with this transformation reached approximately 2–4 wt%.

In the temperature range of approximately 650–750 °C, the TG curve showed a sharp mass decrease of approximately 4–6 wt%, which coincided with the pronounced endothermic effect in the DTA trace. This thermal phenomenon is interpreted as the decomposition of residual carbonate phases, indicating that decarbonization was not completed during the pre-calcination stage at 600 °C.

At temperatures above 750 °C, no significant mass loss was detected, but weak exothermic effects were detected in the DTA curve in the 800–950 °C range. These thermal reactions are associated with structural rearrangement processes and the onset of crystallization of new mineral phases, including the formation of spinel-type compounds and low-temperature calcium silicate structures.

The total mass loss determined from EG data was approximately 8–12 wt.%, which corresponds

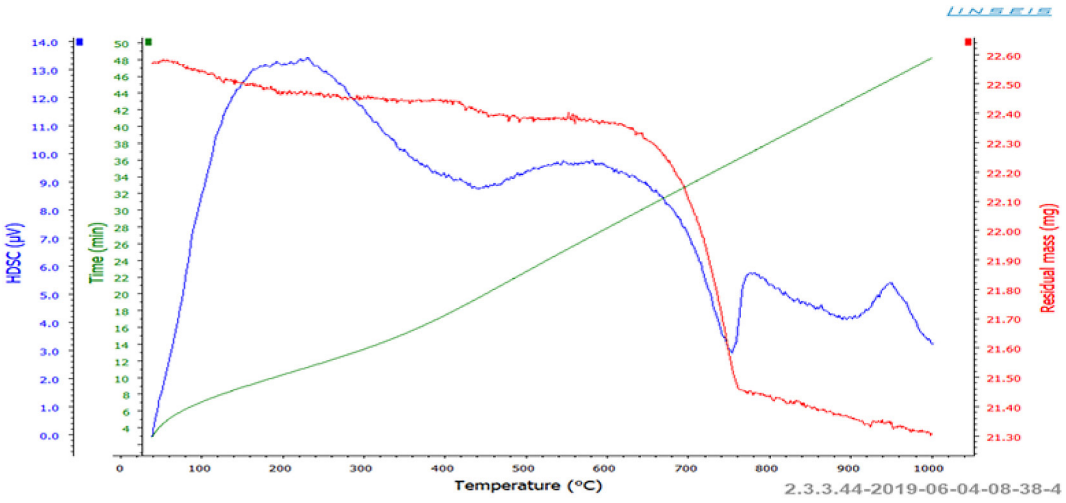


**Figure 2.** DTA/TG curves of the aluminosilicate clinker fired at 600 °C

to the temperature behavior characteristic of low-temperature activated aluminosilicate precursors.

## FTIR analysis and discussion of aluminosilicate clinker at 600 °C

The structural characteristics of the optimum aluminosilicate clinker sample fired at 600 °C were studied by Fourier transform infrared spectroscopy (FTIR), and the resulting spectrum is shown in Figure 3. The spectrum exhibits absorption bands characteristic of a partially amorphous aluminosilicate system, reflecting the incomplete nature of thermal activation at this firing temperature. The broad absorption band observed in the high-frequency region of approximately 3400–3600 cm−1 is attributed to stretching vibrations of hydroxyl (O–H) groups associated with the presence of adsorbed water and residual structural hydroxyl species. The persistence of this band confirms that dehydroxylation of the aluminosilicate framework remained incomplete at 600 °C, which is consistent with the DTA/TG observations.

The band detected in the 1600–1650 cm−1 region is due to the rocking vibrations of molecularly adsorbed water, providing further evidence of the retention of bound moisture within the clinker microstructure at this stage of heat treatment.

The most intense and spectrally broad absorption feature, observed in the 950–1100 cm−1 range, corresponds to asymmetric stretching vibrations of the Si–O–Si and Si–O–Al bonds that make up the aluminosilicate network. The shift of the band maximum toward lower wavenumbers compared to crystalline quartz indicates the formation of a disordered amorphous aluminosilicate phase with a metakaolin-like structural character, in which the long-range crystalline order of the precursor minerals is disrupted.

The absorption bands observed in the 700–800 cm−1 range are attributed to symmetrical stretching vibrations of Si–O, as well as to the possible contribution of residual crystalline quartz phases that were not fully transformed during annealing at 600 °C. The bands observed in the 450–600 cm−1 range are due to deformation (bending) vibrations of the Si–O–Si and Al–O–Si bonds, characteristic of the condensed structure of the silicate framework.

Notably, weak absorption signatures detected in the 1400–1500 cm−1 region are attributed to vibrational modes of carbonate groups ($CO_3^{2-}$), confirming the DTA/TG evidence of incomplete decarbonization of the limestone-derived component at a firing temperature of 600 °C. The simultaneous identification of residual hydroxyl, moisture, and carbonate signatures together indicates that 600 °C represents a thermally intermediate activation state, at which significant structural reorganization has begun, but full phase maturation has not yet been achieved.

## SEM analysis of aluminosilicate clinker at 600 °C

The microstructural characteristics of an optimal aluminosilicate clinker sample fired at 600 °C were studied using SEM, and the resulting micrograph is shown in Figure 4.

The micrograph reveals a heterogeneous microstructure consisting of irregularly shaped particles with a relatively loose and porous

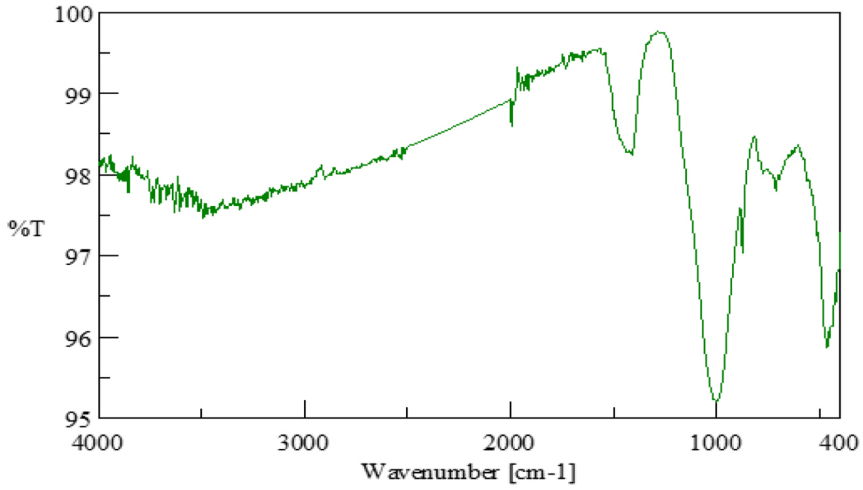


**Figure 3.** FTIR spectrum of the aluminosilicate clinker sample fired at 600 °C

spatial arrangement. Aggregation of small particles into agglomerates of varying sizes is observed, a morphological feature indicating an early stage of structural transformation of the solid occurring during heat treatment at this temperature. The particle surfaces appear distinctly rough and topographically heterogeneous, reflecting the coexistence of partially reacting and non-reacting phases in the clinker matrix, as well as the lack of complete sintering at 600 °C.

The observed microstructural characteristics are consistent with ongoing dehydration and dehydroxylation processes, as revealed by DTA/TG and FTIR analysis, confirming that thermal activation at 600 °C causes significant physicochemical reorganization of the aluminosilicate structure without achieving complete compaction. The next experiments were devoted to the comprehensive analysis of aluminosilicate clinker obtained by firing at 1000 °C.

## XRF analysis of aluminosilicate clinker fired at 1000 °C

To gain a deeper understanding of the structure of the aluminosilicate clinker, XRF and XRD analyses were performed on the sample after thermal treatment at 1000 °C (Figures 5, 6). X-ray fluorescence (XRF) analysis performed using a Rigaku spectrometer showed that the aluminosilicate clinker fired at 1000 °C is characterized by a multicomponent chemical composition with a predominance of silicon, aluminum, and calcium.

The spectrum clearly exhibits intense Si-Kα and Al-Kα peaks, indicating the preservation of the aluminosilicate matrix as the main structure-forming phase. Compared with the sample fired at 600°C, an increase in the relative intensity of Ca-Kα peaks is observed, indicating a more active participation of calcium-containing phases in the clinker formation process.

The increased calcium content (up to ~25 wt.%) compared with the low-temperature sample indicates the development of interaction processes between $SiO_2$, $Al_2O_3$, and CaO, leading to the formation of calcium-containing silicate and aluminate phases. This suggests the initial formation of clinker minerals.

The decrease in relative aluminum content accompanied by an increase in calcium may be associated with the redistribution of Al within calcium–aluminosilicate phases (e.g., $C_2AS$, $C_3A$-like structures). Iron ($Fe_2O_3$) is present in stable amounts (3–7 wt.%) and is likely incorporated into solid solutions of alumina–ferrite phases, contributing to a reduction in the melting temperature of the system.

Alkali elements ($K_2O$, $Na_2O$) remain at levels up to ~5 wt.% and act as mineralizers, promoting the formation of a liquid phase at elevated temperatures.

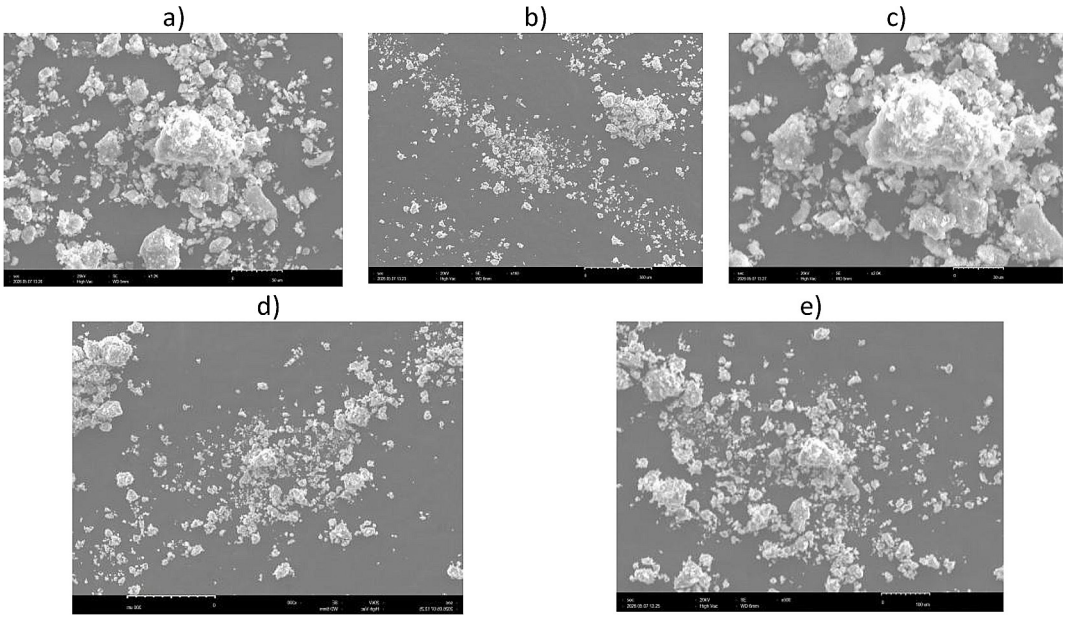


**Figure 4.** SEM image of the aluminosilicate clinker sample fired at 600 °C

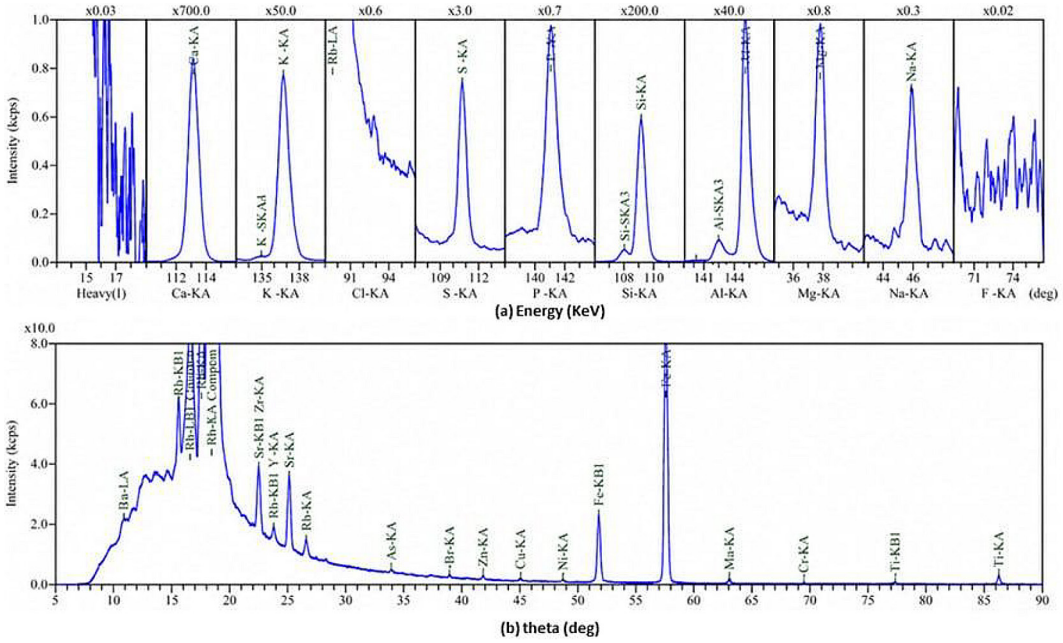


**Figure 5.** Results of X-ray fluorescence (XRF) analysis of aluminosilicate clinker obtained by firing at 1000 °C

## XRD analysis of aluminosilicate clinker fired at 1000 °C

X-ray diffraction analysis of a sample fired at 1000 °C confirmed the formation of well-defined crystalline phases, indicating significant structural rearrangement of the material (Figure 6).

The most intense diffraction peaks in the 2θ range ≈ 20–35° correspond to the aluminosilicate and calcium silicate phases. Quantitative phase analysis was performed using the WPPF method, ensuring reliable phase identification with compatibility parameters of Rwp = 5.72%, Rp = 4.41%, and S = 1.197.

Comparison of the experimental diffraction pattern with reference profiles from the ICDD PDF database revealed the presence of four crystalline phases. Peaks at 2θ ≈ 22.0–22.5°, 27.8–28.2°, 30.0–30.5°, and 32.0–32.5° correspond to andesine (plagioclase aluminosilicate structure), which was identified as the dominant phase with a mass fraction of 55 wt%. This confirms the preservation and recrystallization of the aluminosilicate matrix during high-temperature annealing. Reflections at 2θ ≈ 20.8°, 26.6°, 36.5°, 50.1° and 59.9° correspond to residual α-$SiO_2$ (alpha silicon oxide) present at 4 wt.%, indicating that the minor

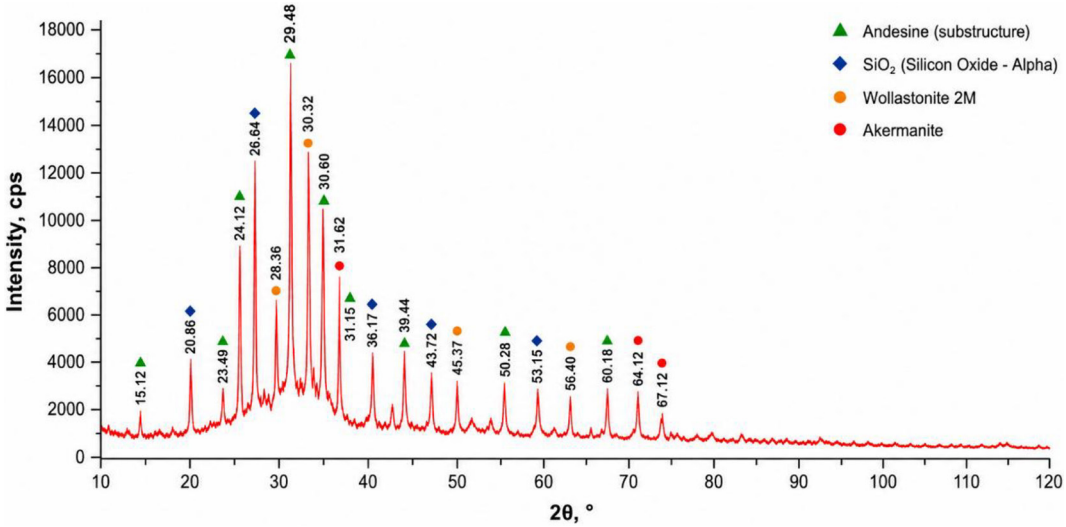


**Figure 6.** XRD pattern of the aluminosilicate binder fired at 1000 °C

fraction of silica did not fully participate in solid-state reactions under the applied firing conditions.

Peaks at 2θ ≈ 26.9–27.2°, 29.0–29.3°, 32.2–32.5°, 39.5–40.0°, and 49.0–49.5° correspond to wollastonite 2M ($CaSiO_3$), which constitutes 33 wt.% of the phase composition. The formation of wollastonite confirms the solid interaction of CaO derived from limestone and $SiO_2$ from aluminosilicate components at elevated temperature. Reflections at 2θ ≈ 31.0–31.5°, 32.5–33.0°, 35.5–36.0°, 41.0–41.5°, and 60.0–61.0° correspond to akermanite ($Ca_2MgSi_2O_7$), which is present at 8 wt.%. The formation of akermanite confirms the participation of MgO in the phase formation and development of complex calcium-magnesium silicate structures at 1000 °C.

## DTA/TG analysis of aluminosilicate clinker fired at 1000 °C

The thermal behavior of the optimal aluminosilicate clinker sample fired at 1000 °C was characterized by simultaneous differential thermal analysis and thermogravimetry (DTA/TG), and the resulting thermogram is shown in Figure 7. Analysis of the DTA curve, combined with the residual mass profile, indicates the progressive formation of a thermally stable aluminosilicate structure in the studied temperature range.

In the temperature range of 150–300 °C, the DTA curve revealed a more pronounced endothermic effect associated with the removal of chemically bound water, dehydration of hydrated intermediate compounds, and the onset of partial decomposition of transition aluminosilicate phases. The TG trace showed a parallel gradual decrease in sample weight during this interval.

In the range of 300–550 °C, progressive restructuring of the clinker framework was evidenced by a gradual weakening of the thermal effect. This stage is interpreted as reflecting the decomposition of residual hydroxyl groups, combustion of microorganism impurities, and the initial development of sintering phenomena in the aluminosilicate system.

In the temperature range of 550–700 °C, a relatively stable region was observed in the thermogram, indicating that the main dehydration processes were nearly complete and a more stable formation of the crystalline phase had begun. Weak residual thermal effects detected in this range are associated with polymorphic phase transformations of aluminosilicate compounds.

At temperatures from 700 to 1000 °C, a gradual evolution of the thermal signal was recorded without significant mass fluctuations, consistent with processes of structural compaction, progressive sintering, and consolidation of the thermally stable aluminosilicate clinker framework. The insignificant mass loss observed at elevated temperatures confirms the high degree of completion of the heat treatment reactions and demonstrates the physicochemical stability of the resulting clinker material.

Compared with the thermal behavior of the sample fired at 600 °C, the thermogram of the sample at 1000 °C shows a significant reduction in the overall mass loss and suppression of the endothermic effects associated with residual hydroxyl and carbonate species, which together

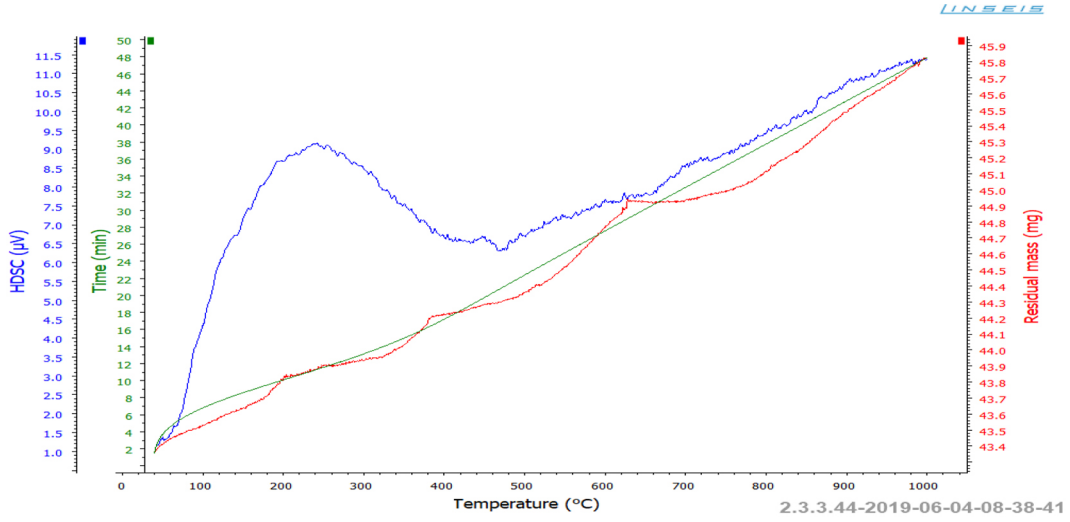


**Figure 7.** Differential thermal analysis of aluminosilicate clinker at 1000 °C

confirm that high-temperature firing promotes more complete phase maturation and structural consolidation of aluminosilicate clinker.

## FTIR analysis of aluminosilicate clinker fired at 1000 °C

The infrared spectrum of the aluminosilicate clinker calcined at 1000 °C is characterized by the presence of intense absorption bands corresponding to silicate and aluminosilicate structural groups, as well as products of high-temperature phase formation.

The most intense absorption band is observed in the range of 1011–993 $cm^{-1}$, which corresponds to the asymmetric stretching vibrations of Si–O–Si and Si–O–Al bonds in the aluminosilicate structure (Figure 8). The high intensity and broadened nature of this band indicate the predominance of a partially amorphized silicate matrix with elements of an ordered structure. The shift of the band maximum toward the region around 1000 $cm^{-1}$ indicates thermal restructuring of the aluminosilicate framework and the formation of calcium-containing silicate phases.

The absorption band in the range of 780–790 $cm^{-1}$ is attributed to the symmetric vibrations of Si–O bonds in the quartz phase. The presence of this signal confirms the preservation of residual α-quartz, which is consistent with the results of X-ray diffraction analysis. The absorption band at 616 $cm^{-1}$ is associated with the deformation vibrations of Si–O–Al and Al–O bonds, characteristic of aluminosilicate structures subjected to high-temperature activation.

The bands in the range of 560–570 $cm^{-1}$ may be attributed to vibrations of calcium silicate compounds, particularly wollastonite-like phases formed during the interaction of CaO and $SiO_2$ at 1000 °C. The low-frequency band at 472 $cm^{-1}$ corresponds to the bending vibrations of Si–O–Si bonds in the silicate framework and indicates the formation of a more ordered structure compared to samples calcined at lower temperatures.

The weak signal observed in the region of 1981 $cm^{-1}$ may be associated with combination vibrations of silicate groups or residual surface carbonate compounds. It should be noted that there are no intense absorption bands in the regions of 3400–3600 $cm^{-1}$ and 1600–1650 $cm^{-1}$, which are characteristic of hydroxyl groups and adsorbed water. This indicates the nearly complete removal of physically and chemically bound moisture during the high-temperature calcination process.

## SEM analysis of aluminosilicate clinker fired at 1000 °C

For a more detailed study of the microstructure of the aluminosilicate clinker sample, microscopic images of the sample were obtained (Figure 9).

The microstructure of the aluminosilicate clinker fired at 1000 °C was investigated using SEM combined with energy-dispersive X-ray spectroscopy (EDS). The obtained results indicate significant structural transformations occurring in the material during the high-temperature firing process.

The SEM image shows the formation of a dense, partially sintered structure with

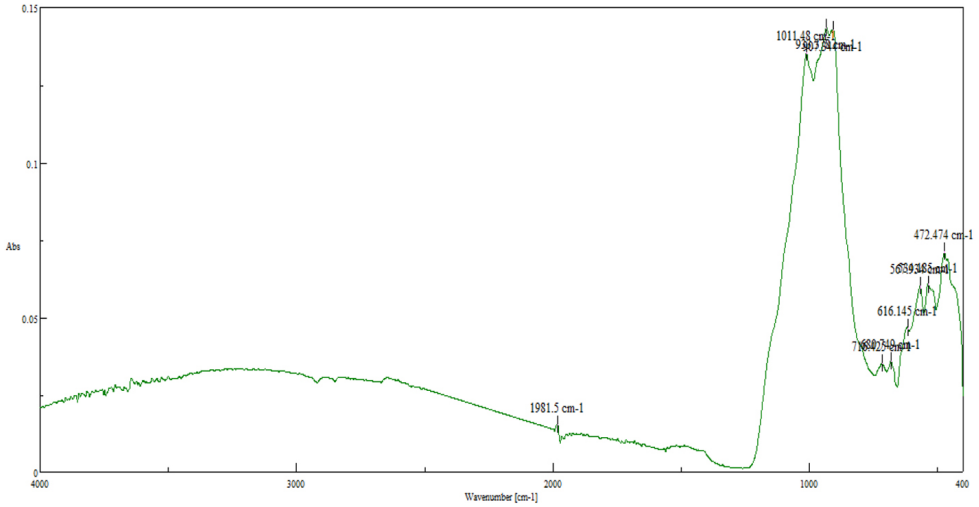


**Figure 8.** FTIR spectrum of the aluminosilicate clinker sample calcined at 1000 °C

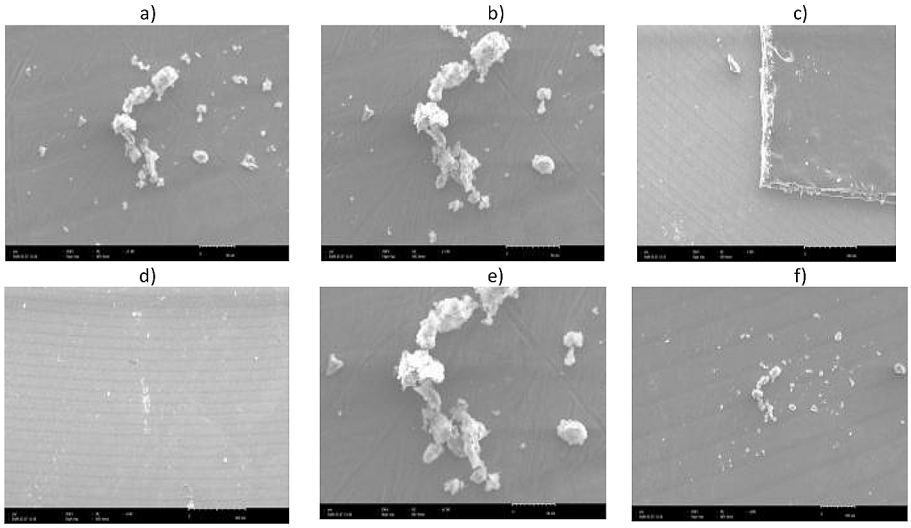


**Figure 9.** SEM image of the aluminosilicate clinker sample fired at 1000 °C

pronounced agglomerated regions. The presence of a heterogeneous surface with local densified zones is observed, indicating the development of solid-state interaction processes and the initial sintering of the aluminosilicate system. Certain areas are characterized by a relatively smooth surface, which may indicate the formation of a glassy phase.

The absence of a pronounced platy morphology of the original clay minerals confirms a profound thermal transformation of the structure at 1000 °C. At the same time, microporous regions and local structural defects are observed, caused by dehydroxylation and the removal of volatile components during the firing process.

The EDS analysis results show that the main elements of the investigated sample are oxygen (O), silicon (Si), aluminum (Al), and calcium (Ca), which form the aluminosilicate matrix of the material. The elevated content of silicon and oxygen confirms the predominance of silicate phases, while the presence of aluminum indicates the preservation of the aluminosilicate structure.

The presence of calcium indicates the formation of calcium silicate compounds, which is consistent with the XRD analysis data, where wollastonite-like phases were identified. In addition, Mg, Fe, K, and Na were detected in the spectrum in smaller amounts. Magnesium is likely involved in the formation of complex calcium–magnesium silicates (akermanite - structures), whereas iron and alkali elements are incorporated into impurity or glassy phases.

**Table 3.** Compressive strength development of the optimal aluminosilicate binder (ASB-3) fired at 1000 °C

| Curing age (days) | Water/binder ratio | Compressive strength, MPa |
|---|---|---|
| 1 | 0.40 | 7.5 |
| 7 | 0.40 | 11.2 |
| 14 | 0.40 | 13.6 |
| 28 | 0.40 | 15.4 |

## Structural changes induced by temperature increase

Comparison of the results obtained at 600 °C and 1000 °C demonstrates a significant influence of firing temperature on the structure of the aluminosilicate clinker. The sample treated at 600 °C retained a predominantly amorphous character, residual hydroxyl-containing groups, and a relatively porous microstructure. In contrast, firing at 1000 °C promoted the completion of dehydration and decarbonization processes, the formation of crystalline phases such as wollastonite and akermanite, and the development of a denser microstructure. The combined XRD, FTIR, DTA/TG, and SEM results indicate a progressive transformation from a partially activated aluminosilicate system to a thermally stable clinker with enhanced structural ordering and phase maturity.

The compressive strength values presented in Table 3 were obtained for ASB-3 samples fired at 1000 °C, as this firing temperature was identified as the most favorable for phase maturation and structural development.

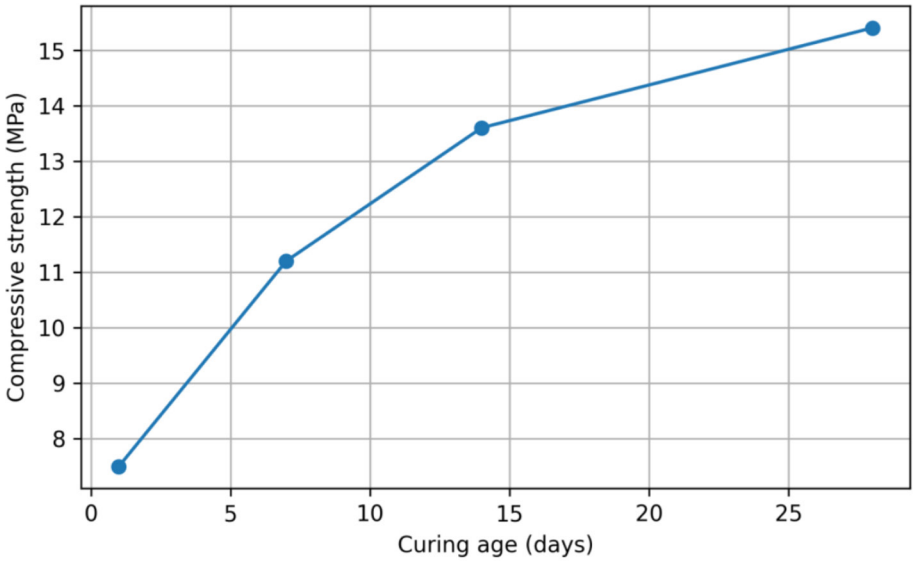


**Figure 10.** Development of compressive strength of the optimal aluminosilicate binder (ASB-3) during curing

The compressive strength of the optimal aluminosilicate binder (ASB-3) increased gradually throughout the curing period. After 1 day of curing, the compressive strength reached 7.5 MPa. Further hydration and structural development resulted in strength values of 11.2 MPa and 13.6 MPa after 7 and 14 days, respectively. The highest strength value of 15.4 MPa was obtained after 28 days of curing.

The observed increase in strength can be attributed to the gradual formation of stable aluminosilicate and calcium-containing phases within the binder matrix. XRD analysis confirmed the formation of wollastonite and akermanite phases, while FTIR analysis revealed progressive structural ordering of the aluminosilicate framework. SEM observations demonstrated a denser and more homogeneous microstructure, which contributed to the improvement of mechanical performance.

As shown in Figure 10, the compressive strength of the optimal aluminosilicate binder (ASB-3) increased steadily throughout the curing period. During the first day, the material developed an initial strength of 7.5 MPa, indicating the beginning of hydration and structural formation processes. A more pronounced increase was observed after 7 days, when the compressive strength reached 11.2 MPa.

Further curing resulted in continued strength development, reaching 13.6 MPa after 14 days and 15.4 MPa after 28 days. The gradual increase in strength indicates the ongoing formation of binding phases and the densification of the aluminosilicate matrix. The obtained results are in good agreement with the physicochemical analyses. XRD results confirmed the formation of calcium-containing aluminosilicate phases, while FTIR analysis demonstrated progressive structural ordering of the aluminosilicate framework. SEM observations revealed a denser microstructure with reduced porosity, which contributed to the improvement of mechanical properties.

Therefore, the optimal aluminosilicate binder (ASB-3) exhibits satisfactory hardening behavior and demonstrates the potential for application as a sustainable binder material produced from local mineral and technogenic raw materials.

## CONCLUSIONS

A comprehensive physicochemical study was conducted to determine the optimal composition of aluminosilicate clinker obtained from kaolin, limestone, ceramic brick waste, and liquid glass, heat-treated at 600 °C and 1000 °C. Based on a comprehensive analysis of XRF, DTA/TG, FTIR, XRD, and SEM/EDS data, the following key conclusions were reached.

The optimal clinker formulation, designated ASB-3, containing 39 wt.% kaolin, 15 wt.% limestone, 30 wt.% ceramic brick waste, and 16 wt.% liquid glass, was determined through systematic composition optimization. This formulation ensures a thermodynamically favorable balance of aluminosilicate and calcium-containing

components, thereby creating the necessary chemical conditions for the development of reactive mineral phases during high-temperature firing.

Heat treatment at 600 °C caused partial activation of the aluminosilicate system. DTA/TG and FTIR analyses collectively revealed incomplete dehydration, dehydroxylation, and decarbonation, as evidenced by the retention of residual hydroxyl groups, adsorbed moisture, and carbonate species ($CO_3^{2-}$). SEM observations confirmed the formation of a heterogeneous, porous, and partially sintered microstructure characteristic of an intermediate state of thermal activation.

Increasing the firing temperature to 1000 °C facilitated extensive phase and structural transformations in the clinker system. X-ray diffraction analysis confirmed the formation of well-defined crystalline phases, including wollastonite ($CaSiO_3$) and akermanite ($Ca_2MgSi_2O_7$), demonstrating advanced solid-state interactions between silica, alumina, and calcium components at elevated temperatures.

Integrated FTIR, DTA/TG, and SEM characterization revealed that clinker fired at 1000 °C exhibits a significantly higher degree of structural ordering, significantly reduced porosity, improved microstructural densification, and superior thermal stability compared to the sample fired at 600 °C. Suppression of residual endothermic effects and insignificant mass loss at high temperatures further confirmed the nearly complete maturation of the aluminosilicate framework.

Among the thermal conditions studied, 1000 °C was identified as the most favorable firing temperature for producing thermally stable aluminosilicate clinker, characterized by increased phase maturity, a well-developed crystalline structure, and excellent microstructural integrity.

The successful use of locally produced kaolin, limestone, and ceramic brick waste as the main raw material component demonstrates the feasibility of developing resource-efficient and environmentally sustainable aluminosilicate binders, which contributes to the reduction of industrial waste and the promotion of circular economy principles in the production of building materials.

## REFERENCES


1. Davidovits, J. (2020). *Geopolymer chemistry and applications* (5th ed.). Geopolymer Institute.
2. Provis, J. L., van Deventer, J. S. J. (2009). *Geopolymers: Structure, processing, properties and industrial applications*. Woodhead Publishing. https://doi.org/10.1533/9781845696382
3. Duxson, P., Fernández-Jiménez, A., Provis, J. L., Lukey, G. C., Palomo, A., van Deventer, J. S. J. (2007). Geopolymer technology: The current state of the art. *Journal of Materials Science, 42*(9), 2917–2933. https://doi.org/10.1007/s10853-006-0637-z
4. Barbosa, V. F. F., MacKenzie, K. J. D., Thaumaturgo, C. (2000). Synthesis and characterisation of materials based on inorganic polymers of alumina and silica. *International Journal of Inorganic Materials, 2*(4), 309–317. https://doi.org/10.1016/S1466-6049(00)00041-6
5. Taylor, H. F. W. (1997). *Cement chemistry* (2nd ed.). Thomas Telford Publishing.
6. Deja, J. (2020). Free lime and clinker reactivity. *Cement and Concrete Research, 130*, 105991. https://doi.org/10.1016/j.cemconres.2020.105991
7. Scrivener, K., Snellings, R., Lothenbach, B. (2018). *A practical guide to microstructural analysis of cementitious materials*. CRC Press.
8. Mindess, S., Young, J. F., Darwin, D. (2003). *Concrete materials science*. Prentice Hall.
9. Schneider, M., Romer, M., Tschudin, M., Bolio, H. (2019). Sustainable cement production—Present and future. *Cement and Concrete Research, 124*, 105779. https://doi.org/10.1016/j.cemconres.2019.105779
10. Komnitsas, K., Zaharaki, D. (2007). Geopolymerisation: A review and prospects. *Minerals Engineering, 20*(14), 1261–1277. https://doi.org/10.1016/j.mineng.2006.11.007
11. Provis, J. L., Palomo, A., Shi, C. (2015). Advances in understanding alkali-activated materials. *Cement and Concrete Research, 78*, 110–125. https://doi.org/10.1016/j.cemconres.2015.04.013
12. Begzhanova, G. B., Yakubzhanova, Z. B., Wang, L., Makhsudova, N. D., Ruzmetova, A. Sh. (2025). Study of the suitability of industrial raw material resources as additives for Portland cement. *Complex Use of Mineral Resources, 341*(2), 71–82. https://doi.org/10.31643/2027/6445.19
13. Kriven, W. M. (2021). Geopolymers and alkali activated materials. *Journal of the American Ceramic Society, 104*(5), 1841–1878. https://doi.org/10.1111/jace.17661
14. Provis, J. L. (2018). Alkali-activated materials. *Cement and Concrete Research, 114*, 40–48. https://doi.org/10.1016/j.cemconres.2017.02.009
15. Fernández-Jiménez, A., Palomo, A. (2003). Characterisation of fly ashes and their reactivity. *Fuel, 82*(18), 2259–2265. https://doi.org/10.1016/S0016-2361(03)00194-7
16. Khadzhiev, A., Atabaev, F. (2023). Influence of silica-containing additives on the physical and mechanical properties of Portland Cement

Co Ltd Karakalpaksement. *E3S Web of Conferences, 401*, 05051. https://doi.org/10.1051/e3sconf/202340105051

17. Iskandarova, M. I., Yakubzhanova, Z. B., Atabaev, F. B., Begzhanova, G. B., Kakurina, L. M., Kahhorov, U., Khadzhiev, A. S. (2022). Development of technology for obtaining Portland cement with new types of composite additives. *AIP Conference Proceedings, 2432*(1), 030014. https://doi.org/10.1063/5.0092064
18. Khadzhiev, A., Atabaev, F., Jumaniyozov, A., Yakubov, Y. (2024). Study on pozzolanic activity of porphyrites of the Karatau deposit. *E3S Web of Conferences, 563*, 02029. https://doi.org/10.1051/e3sconf/202456302029
19. Khadzhiev, A., Atabaev, F., Tursunova, G. (2024). Influence of sandstone on physical and chemical processes of interaction of components and genetic formation of cement composite. *E3S Web of Conferences, 563*, 02027. https://doi.org/10.1051/e3sconf/202456302027
20. Iskandarova, M., Atabaev, F., Tursunova, G., Tursunov, Z., Khadzhiev, A. (2025). Composite Portland cements: Innovations and future directions in cement technology. *Innovative Infrastructure Solutions, 10*, Article 352. https://doi.org/10.1007/s41062-025-02067-x
21. Khadzhiev, A., Abdullaev, M., Yakubov, Y., Jumaniyozov, J. (2025). The effect of hybrid mineral additives on the genetic formation and physico-chemical processes of cement composites. *E3S Web of Conferences, 633*, 08003. https://doi.org/10.1051/e3sconf/202563308003
22. Iskandarova, M. I., Atabaev, F. B., Khadzhiev, A. S. (2026). Utilization of natural silicate rocks to reduce the carbon footprint in the cement industry. *Kompleksnoe Ispolzovanie Mineralnogo Syra = Complex Use of Mineral Resources, 338*(3), 40–50. https://doi.org/10.31643/2026/6445.27
23. Atabaev, F. B., Aripova, M. Kh., Khadzhiev, A. Sh., Tursunova, G. R., Tursunov, Z. R. (2027). Effect of multicomponent mineral additives on the microstructure and strength of composite cement. *Kompleksnoe Ispolzovanie Mineralnogo Syra = Complex Use of Mineral Resources, 340*(1), 45–57. https://doi.org/10.31643/2027/6445.05
24. Van Jaarsveld, J. G. S., van Deventer, J. S. J. (1999). Effect of metal contaminants on the formation and properties of waste-based geopolymers. *Cement and Concrete Research, 29*(8), 1189–1200. https://doi.org/10.1016/S0008-8846(99)00104-3
25. Rickard, W. D. A., Williams, R., Temuujin, J., van Riessen, A. (2011). Assessing the suitability of three Australian fly ashes as geopolymer precursors. *Materials and Design, 32*(3), 1632–1639. https://doi.org/10.1016/j.matdes.2010.12.022
26. Ruzmetova, A., Babaev, Z., Yunusov, M. (2023). Preparation and investigation of a heat-resistant binder with a metakaolin additive made of Aral Sea raw materials. *Refractories and Industrial Ceramics, 64*(4), 383–387. https://doi.org/10.1007/s11148-024-00857-x
27. Lesovik, V. S., Zagorodniuk, L. Kh., Madaminov, D. K., Yunusov, M. Yu., Ruzmetova, A. Sh., & Djumaniyazov, Z. B. (2026). Dune sands from the Kushkupyr deposit (Uzbekistan) for the production of sodium silicate based on a microsilica–dune sand–caustic soda system. *Glass and Ceramics, 82*(9–10), 48–56.
28. Temuujin, J., van Riessen, A., Williams, R. (2009). Influence of calcium compounds on the mechanical properties of fly ash geopolymer pastes. *Journal of Hazardous Materials, 167*(1–3), 82–88. https://doi.org/10.1016/j.jhazmat.2009.03.065
29. Liu, X., Liu, X., Hu, Y. (2018). Investigation of the thermal behaviour and decomposition kinetics of kaolinite. *Clay Minerals, 53*(4), 613–624. https://doi.org/10.1180/clm.2018.34
30. Duxson, P., Lukey, G. C., van Deventer, J. S. J. (2007). The thermal evolution of metakaolin geopolymers. Part 2: Phase stability and structural development. *Journal of Non-Crystalline Solids, 353*(22–23), 2186–2200. https://doi.org/10.1016/j.jnoncrysol.2007.02.040
31. Bell, J. L., Driemeyer, P. E., Kriven, W. M. (2009). Formation of ceramics from metakaolin-based geopolymers: Part I. *Journal of the American Ceramic Society, 92*(1), 1–8. https://doi.org/10.1111/j.1551-2916.2008.02831.x
32. Bell, J. L., Driemeyer, P. E., Kriven, W. M. (2009). Formation of ceramics from metakaolin-based geopolymers: Part II. *Journal of the American Ceramic Society, 92*(3), 607–615. https://doi.org/10.1111/j.1551-2916.2008.02832.x
33. Bernal, S. A., Rodríguez, E. D., Mejía de Gutiérrez, R., Provis, J. L. (2011). Mechanical and thermal characterisation of geopolymers based on silicate-activated metakaolin/slag blends. *Journal of Materials Science, 46*(16), 5477–5486. https://doi.org/10.1007/s10853-011-5596-9
34. Yao, X., Zhang, Z., Zhu, H., Chen, Y. (2009). Geopolymerization process of alkali-metakaolinite characterized by SEM and XRD. *Colloids and Surfaces A: Physicochemical and Engineering Aspects, 336*(1–3), 57–63. https://doi.org/10.1016/j.colsurfa.2008.07.037
35. Zuda, L., Rovnaníková, P. (2007). Thermal properties of geopolymer materials after exposure to elevated temperatures. *Cement and Concrete Composites,29*(8),579–585. https://doi.org/10.1016/j.cemconcomp.2006.07.009
36. Kong, D. L. Y., Sanjayan, J. G. (2010). Effect of elevated temperatures on geopolymer paste,

mortar and concrete. *Cement and Concrete Research, 40*(2), 334–339. https://doi.org/10.1016/j.cemconres.2009.10.017

37. Kong, D. L. Y., Sanjayan, J. G. (2008). Damage behavior of geopolymer composites exposed to elevated temperatures. *Cement and Concrete Composites, 30*(10), 986–991. https://doi.org/10.1016/j.cemconcomp.2008.08.001
38. Rovnaník, P. (2010). Effect of curing temperature on the development of hard structure of metakaolin-based geopolymer. *Construction and Building Materials, 24*(7), 1176–1183. https://doi.org/10.1016/j.conbuildmat.2009.12.023
39. White, C. E., Provis, J. L. (2014). Structural studies of geopolymer gels by advanced spectroscopic methods. *Journal of Non-Crystalline Solids, 386*, 61–72. https://doi.org/10.1016/j.jnoncrysol.2013.08.021
40. Buchwald, A., Hilbig, H., Kaps, C. (2007). Alkali-activated metakaolin-slag blends—Performance and structure in dependence of their composition. *Cement and Concrete Research, 37*(10), 1381–1390. https://doi.org/10.1016/j.cemconres.2007.06.006
41. Heah, C. Y., Kamarudin, H., Al Bakri, A. M. M., Bnhussain, M., Luqman, M., Nizar, I. K., Ruzaidi, C. M., Liew, Y. M. (2012). Study on solids-to-liquid and alkaline activator ratios on kaolin-based geopolymers. *Construction and Building Materials, 35*, 912–922. https://doi.org/10.1016/j.conbuildmat.2012.04.102
42. Zhang, Z., Provis, J. L., Reid, A., Wang, H. (2014). Geopolymer foam concrete: An emerging material for sustainable construction. *Cement and Concrete Composites, 56*, 113–127. https://doi.org/10.1016/j.cemconcomp.2014.03.009
43. Tchakouté, H. K., Rüscher, C. H. (2017). Mechanical and microstructural properties of geopolymer cements based on natural aluminosilicate materials. *Case Studies in Construction Materials, 6*, 95–104. https://doi.org/10.1016/j.cscm.2017.03.001
44. Tchadjie, L. N., Ranjbar, N. (2018). Enhancing the reactivity of aluminosilicate materials toward geopolymer synthesis. *Journal of Materials Research and Technology, 7*(4), 439–459. https://doi.org/10.17159/2411-9717/2018/v118n1a3
45. Makarova, L. N., Shmidt, V. V., Ismagilova, A. V., Makarov, V. V. (2024). Properties and phase composition of cement mortars. *E3S Web of Conferences, 633*, 01016. https://doi.org/10.1051/e3sconf/202463301016
46. Yaqubov, Y. Kh., Matchanov, S. K., Ruzmetova, A. Sh. (2023). Khodjakul kaolins of Uzbekistan: Composition, physical and chemical properties, and processing methods. *Obogashchenie Rud, 5*, 27–32. https://doi.org/10.17580/or.2023.05.06
47. Matchanov, S. K., Ruzmetova, A. Sh., Yakubov, Y. Kh. (2025). Experiments on bleaching of kaolin from the Khodjakulskoye deposit. *E3S Web of Conferences, 633*, 02008.
48. Matchanov, S. K., Ruzmetova, A. Sh., Yakubov, Y. Kh., Matchanov, S. Sh., Jumaniyazova, K. Q. (2025). Research on kaolin bleaching of Khojakul deposit. *AIP Conference Proceedings, 3304*, 040033. https://doi.org/10.1063/5.0269851
49. Mintsaev, M. S., et al. (2022). Structural formation of alkali-activated materials based on thermally treated marl. *Materials, 15*(19), 6694. https://doi.org/10.3390/ma15196694